Asian Journal of Chemistry; Vol. 34, No. 9 (2022), 2415-2423

ASIAN JOURNAL OF CHEMISTRY

https://doi.org/10.14233/ajchem.2022.23607

Green Synthesis of Cerium Oxide Nanoparticles, Antibacterial Studies and as Catalyst for the Conversion of Cotton Seed Oil into Biodiesel

G.E. Rudreshappa[1], Madhu Chennabasappa[2,*], S. Sreenivasa[3,4], S. Vijaya Kumar[5], K.V. Yatish[6], G. Nagaraju[1], H.M. Suresh Kumar[2] and D.B. Aruna Kumar[3,*]

[1]Department of Chemistry, Siddaganga Institute of Technology, Tumakuru-572103, India
[2]Department of Physics, Siddaganga Institute of Technology, Tumakuru-572103, India
[3]Department of Studies and Research in Chemistry, Tumkur University, Tumakuru-572103, India
[4]National Assessment and Accreditation Council (NAAC), Chandra Layout Extension II Stage, Naagarabhaavi, Bengaluru-560072, India
[5]Department of Pharmacology, Sree Siddaganga College of Pharmacy, B.H. Road, Tumakuru-577202, India
[6]District Biofuel Research and Information Centre, Mechanical Engineering Department, Siddaganga Institute of Technology, Tumakuru-572103, India

*Corresponding authors: E-mail: madhuc@sit.ac.in; nirmaldb@rediffmail.com

Received: 4 November 2021; *Accepted*: 16 July 2022; *Published online*: 19 August 2022; AJC-20941

Cerium oxide nanoparticles were synthesized by employing solution combustion method using environmental friendly, polypeptide and acids rich, *Butea monosperma* seed powder as fuel. Phase purity, crystallite size were determined from X-ray diffraction (XRD). The trace amount of organic species attached to the surface of the nanoparticles is identified using Fourier transform infrared spectroscopy (FTIR). Morphological studies are performed on SEM and the particle shape-size distributions are studied using TEM. Electron diffraction on the nanoparticles revealed good crystallinity of the synthesized samples. Band gap increased with decreasing particle size was confirmed from the diffuse reflectance spectroscopy (DRS). White light luminescence capabilities of CeO_2 nanoparticles were studied using photoluminescence spectroscopy. *In vitro* antibacterial activity studies to determine the zone of inhibition (ZOI) and catalytic property for the conversion of cotton seed oil into biodiesel were performed.

Keywords: Cerium oxide nanoparticles, *Butea monosperma*, Photoluminescence, Biodiesel.

INTRODUCTION

During recent days, worldwide transportation sector is almost entirely dependent on petroleum derived fuels. Unfortunately, petroleum based products are one of the main causes of anthropogenic CO_2 emission to the atmosphere [1-4]. CO_2 emission-free fuels such as sustainable and renewable energies are of great importance to meet the growing demand in domestic and commercial transportation. Biodiesel is one of the greener alternatives for fossil fuels. Biodiesel generation requires catalysts, which are cost effective with greater efficiency.

Cerium exists as a free metal, crystallizes in a cubic fluorite structured and does not show any crystallographic change from room temperature to its melting point (795 ºC) [1]. Nanoceria (cerium oxide nanoparticles) also exist in between Ce^{III} and Ce^{IV} valence states and contain oxygen vacancies that allow the nanoparticles to act as regenerative catalyst [2]. CeO_2 adopts a fluorite type $Fm\bar{3}m$ crystal structure in which each metal cation is surrounded by '8'oxygen atoms. Band gap of pure ceria is approximately 3.19 eV. Crystal defects or impurities implanted due to size reduction can transform the material into a good n-type semiconductor and also induce mild magnetism [5]. Bulk CeO_2 is an ionic covalent compound or covalent insulator. It is an attractive insulating material because of its excellent chemical stability, high relative permittivity and close lattice match with silicon. It has found applications such as capacitors and buffer layers of superconducting materials [6].

Ceria, either in its pure form or doped with different cations (Ca^{2+}, Mg^{2+}, Sc^{2+}, Y^{3+}, Zr^{4+}, *etc*.). are used in numerous applications including gas sensors, electrode materials for solid-oxide fuel cells, oxygen pumps, amperometric oxygen monitors and catalytic support for automobile exhaust system. Its ability

to undergo a facile conversion between +4 and +3 formal oxidation states helps in catalysis used to reduce the emissions of CO, NOx and hydrocarbons from automobile exhaust. Atomic size of Ce^{3+} is 1.14 Å and Ce^{4+} is 0.97 Å. Oxygen vacancies and structural imperfections as well as surface defects can be present resulting strain in the lattice. Ceria nanoparticles with less than 10 nm have higher electronic conductivity than bulk ceria. Bulk ceria is able to absorb and store oxygen, the same is true with CeO_2 nanoparticles. Movement of 'H' atoms towards 'O' sites forms hydroxyl series in CeO_2, which helps in the removal of oxygen during reduction process and generates Ce^{3+} cations [7].

CeO_2 nanoparticles absorb 'CO' and decompose 'NO' and SO_2 at room temperature. Size of CeO_2 particles can be varied from 4-7 nm inducing the local distortions on the cubic lattice structure as a consequence of defects in the oxide lattice. CeO_2 nanoparticles are used in catalysis, electrochemistry, photochemistry and material science [8-10]. The nanoparticles have been synthesized by different techniques such as hydrothermal, sonochemical, mechanochemical, combustion synthesis, sol-gel, semi-batch reactor, micro-emulsion and spray pyrolysis [6,11,12]. Solution combustion synthesis (SCS) has an edge over other methods and widely adopted technique to synthesize nanomaterials, especially for oxides, because of its simplicity, energy and time effectiveness and low cost [13]. The general difficulty encountered in SCS is the controllability over phases and morphologies of the products, which arises from the inherent rapid and uncontrollable combustion procedure. One can find reports in literature on novel adopted approaches to control the phase and morphology of the synthesized materials through solution-combustion synthesis of nanomaterials [14-16].

Green synthesis is highlighted as one of the cost efficient alternative to the conventional physical or chemical methods of metal nanoparticles synthesis and would also be suitable for large scale production. In recent years, it is explored that plant extracts can act as reducing and/or capping agents for the synthesis of nanoparticles and is more advantageous with reference to chemical, microbial synthesis [17,18]. In this regard, synthesis of CeO_2 nanoparticles using different extracts such as water melon juice as fuel, *Tamarindus indica* fruit, *Aloe barbadensis miller gel* as, Leucasaspery and other along with cerium(III) nitrate are reported [19-21]. During last couple of decades, the nanoparticles have gained much importance in the catalytic process related to the societal as well as environmental point of view thanks to their inherent properties such as selectivity, durability, activity and recoverability. Nanoparticles based catalysts have smaller particles leading to the reaction efficiency and higher surface to volume ratio are higher thereby reducing the required quantity of catalyst in a given reaction. Currently, the nanocatalysts such as Al-Sr [22], Ca/Fe_3O_4@SiO_2 [23], mixed oxide SiO_2/ZrO_2 [24], La_2O_3 [25], ZnO [26], Fe(II)-ZnO [27] and Cu-ZnO [28] are used for the biodiesel synthesis.

Every part of the *Butea monosperma* plant is species of *Butea* with great medical importance from ancient times and is widely grown in India, Ceylon and Burma. It is commonly known as Palash in the field of Ayurveda, the Indian medicine. The seed extract obtained using different alcohol groups is proven for its effectiveness in treatment of hormone imbalance, antifertility effect, anthelmintic effect, anti-hyperglycemic and anti-hyperlipidemic. Seeds are rich in polypeptidase, proteinase, lypolytic enzymes, proteolytic along with minor components of palasonin, nitrogenous acid, mixed fatty acids and unsaponifiable matter. Hence, it is believed that the seed to be a good source of reducing agent thereforth we have selected *Butea monosperma* seed as fuel in present study [29-31]. Ceria has potential in particular for energy related applications and catalytic application in environmental view point [32]. Herein, the green synthesis of cerium oxide (ceria) nanoparticles is conducted using $Ce(NO_3)_3{\cdot}6H_2O$ (m.w. = 434.22), *Butea monosperma* seed as fuel and distilled water by solution combustion method at 500 ºC. Structural, morphological and physical properties of the sample are studied using XRD, FTIR, UV-visible, DRS studies, photoluminescence and SEM/TEM analysis. The synthesized nano-ceria were tested for their biological activities using disc diffusion assay to evaluate the antibacterial property. They are also used as catalyst for the conversion of cotton seed oil into biodiesel.

EXPERIMENTAL

Preparation of fuel from *Butea monosperma* seed: Fresh *Butea monosperma seeds* were collected, washed several times using tap water followed by AR grade distilled water. They were shade dried for two days at room temperature before powdering using blender. The resulting powder are used for synthesis of CeO_2 nanoparticles.

Synthesis of CeO_2 nanoparticles: Cerium nitrate hexahydrate (1.0 g) and finely powderd *Butea monosperma* seed (40 mg) were added in to 20 mL of distilled water in a beaker and transferred into a silica crucible. The crucible was placed in a preheated muffle furnace at 500 ºC for 10 min. The crucible was taken out from the muffle furnace and kept in air for 10 min. Again the crucible was placed in the muffle furnace for calcinations at 500 ºC for 3 h and allowed to cool. The same procedure was repeated with 60 and 80 mg of fine powder of *Butea monosperma* seed as fuel. The overall reaction can be represented as follows:

$$Ce(NO_3)_3{\cdot}6H_2O\ (1\ g) + \textit{Butea monosperma}\ (40\ mg) + H_2O \longrightarrow CeO_2\ NPs + H_2O + CO_2 + NO_2$$

Cerium oxide nanoparticles (NPs) obtained above were subjected for characterization and evaluated for photocatalytic, photoluminescence and antibacterial activities. It was also subjected for catalysis studies for converting cotton seed oil into biodiesel applications.

Characterization: The samples were characterized using powder X-ray diffractometer (Rigaku Smart lab X-ray diffractometer using copper radiation with Ni filter). X-ray diffraction at 40 kV was used to estimate the crystallite sizes. The XRD pattern was scanned from 10-80º using Cu$K\alpha$ radiation. Metal oxide bond stretching frequencies were analyzed by FTIR spectrometer (Bruker-alpha). The UV measurements on the samples were measured using UV-visible absorbance and reflectance spectrophotometers (Agilent Cary-60 and LABINDIA

UV3092 spectrophotometer). The morphologies of the synthesized CeO_2 nanoparticles were scanned using scanning electron microscopy (Hitachi-7000 Table top). Electron diffraction rings and HRTEM of CeO_2 crystallites were obtained using transmission electron microscopy (JEOL-3010) attached with EDX present at the SAIF-STIC facility, Cochin, India.

Surface area studies: Surface area are measured using BELSORP-mini, Japan BET surface area analyser, nitrogen gas was used as the adsorption and desorption medium by the known quantity of the sample in a constrained volume cell.

Photocatalytic activity: The photocatalytic activity of the synthesized cerium oxide nanoparticles was evaluated by degradation of methylene blue in an aqueous solution at room temperature using a 120 W mercury lamp as radiation source as described earlier [33]. For probing catalysis, 50-200 mg of synthesized nanoparticles as photo catalyst was added to 100 mL of methylene blue solutions of different concentrations (5-20 ppm) in a batch reactor with a gap of 18 cm between the radiation source and the reactor. The solution was continuously stirred in the dark chamber for about 30 min to ensure the complete organization of an adsorption as well as the desorption equilibrium between the methylene blue dye and photocatalyst. Then, 2 mL volume of the suspension was withdrawn from the above solution at a regular sequence of 30 min intervals. After the removal of the photocatalyst from the solution by centrifugation, the concentration of left over aqueous solution was monitored using UV-visible spectrophotometer at a fixed wavelength of 664 nm and the % degradation of methylene blue dye has been calculated based on the principle of Beer-Lambert's law.

Photoluminescence studies: Photoluminescence (PL) studies were recorded using fluorescence spectrophotometer (Agilent Cary Eclipse fluorescence spectrometer) using Xe lamp with an excitation wavelength of 398 nm. PL studies are aimed at determining the effectiveness of trapping, migration and transfer of charge carriers and to understand the fate of $^{-}e - h^{+}$ pairs in semiconductors.

Biodiesel production and evaluation of fuel properties: The percentage of free fatty acid present in the cotton seed oil was determined by volumetric method and found to be 1.19%. The FFA content of cotton seed oil was found to be less than 2%. Hence, single stage base transesterification was much suitable for cotton seed oil methyl ester/biodiesel production as described earlier [34]. Oil (200 g) was taken in a three neck round bottom flask equipped with condenser and placed on a mechanical stirrer. Initially, oil was preheated at 60 ºC, then 2 wt.% of CeO_2 nanoparticles and 12:1 methanol to oil molar ratio mixture was added to the oil. Then the reaction was carried out for a period of 2 h at 65 ºC and by maintaining a stirring speed of at 650 rpm to ensure homogeneous reaction. After completion of the reaction, three phases are obtained: upper phase (biodiesel), middle phase (glycerol) and lower phase (catalyst). Finally, biodiesel was separated from the methanol by distillation at 65 ºC.

Antibacterial activities: The antibacterial activities of CeO_2 nanoparticles were studied by disc diffusion method using *Escherichia coli*, *Staphylococcus aureus* and *Pseudomonas aeruginosa*. The zone of inhibition (ZOI) in mm was used to quantify the antibacterial activity. The synthesized CeO_2 nanoparticles along with *Escherichia coli*, *Staphylococcus aureus* and *Pseudomonas aeruginosa* were used to determine the ZOI using the Agar disc-diffusion assay [35,36]. The stock solutions of CeO_2 nanoparticles was prepared by weighing exactly 10 mg and the total volume was made up to 10 mL to get 1 mg/mL solution, further it was diluted to get desired concentration in mcg/mL. Standard ciproflaxcin was also prepared using same protocol.The bacterial cultures were grown in the nutrient broth overnight to attain the ~ 10^6 CFU. Each bacteria culture (100 µL) was spread on the agar plates and incubated at 37 ºC for 24 h test and standard studies were also carried out simultaneously.

RESULTS AND DISCUSSION

X-ray diffraction studies: The X-ray diffraction studies confirmed the polycrystalline nature of cerium oxide nanoparticles. Intense peaks were obtained are indexed to 111, 200, 220, 311 Bragg's lattice. The peaks are in well accordance with JCPDS No. 1-800 of CeO_2 crystal and belong to cubic system. The synthesized nanoparticles studied reveal that by varying the seed concentration between 40 to 80 mg shows that the peaks get narrower with increasing seed concentration suggesting the increase in the amount of heat released during combustion that increases the crystallite size. From the full-width at half maxima (FWHM) of the calculated curves, we obtain the crystallite size, dislocation density and strain and they are summarized in Fig. 1 [6]. The broadening of the XRD peaks indicates ultrafine nature of the CeO_2 crystallites. Average crystallite size of CeO_2 nanoparticles calculated for the four most intense peak from Debye-Scherer's equation:

$$D = \frac{k\lambda}{\beta\cos\theta}$$

where k = 0.94 as ceria crystallize in cubic symmetry and the particles are assumed to be spherical, 'D' is crystal size, λ is the wave length of X-ray radiation (1.5428 Å), β is the full width at half the maximum intensity (FWHM) of diffraction peak and θ is the scattering angle. The dislocation density $\delta = d = \frac{1}{D^2}$ and the micro-strain $\varepsilon = \frac{\beta}{4\tan\theta}$ are also calculated. Crystallite size was found to increase from 12 to 15 nm with increase of seed concentration from 40 to 80 mg whereas the dislocation density and the microstrain decrease with increasing crystallite size, suggesting that the particle size variation induces the strain and vacancies in the crystallite lattice. Further, profile fitting on these samples revealed the decrease of lattice parameter with increasing fuel concentration.

Rietveld refinement analysis on the synthesized nanoparticles was performed using FullProf suite program, considering space group as $Fm\bar{3}m$ (No. 186) for cubic structure. Pseudo-voigt function is used to fit the peak parameters of the XRD data. The refinement parameters such as occupancy, atomic functional positions for Ce and O atoms of CeO_2 nanoparticles were studied. The obtained results are in good agreement with

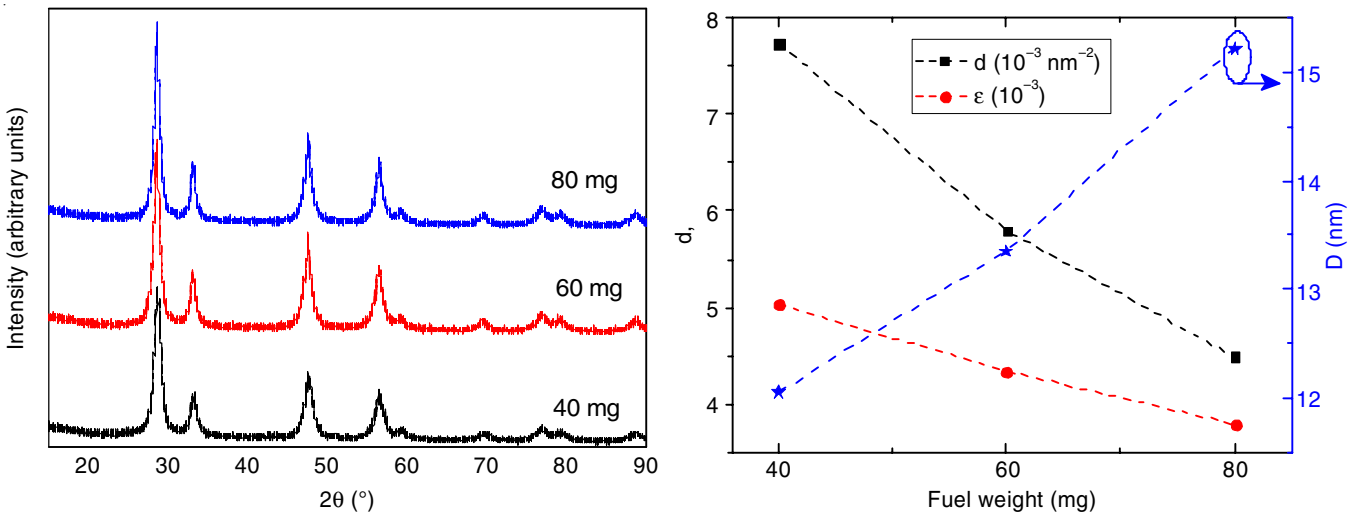

Fig. 1. X-ray diffraction pattern for nanoparticles obtained using variant fuel ratio (on left) and their crystallite size (D), dislocation-density (d) and micro-strain (å) obtained from the XRD (on right)

the reported once. Lattice parameter, bond distances for CeO_2 NPs prepared by solution combustion method were determined from the Rietveld refinement and the results are tabulated in Table-1.

FTIR studies: *Butea monosperma* seed are rich in polypeptidase, proteinase and offer high entropy on decomposition. This entropy is channelized as the fuel in the formation of cerium oxide from cerium nitrate. The purity of the synthesized nanoparticles is addressed in terms of phase purity and at the same time, the residual components of the fuel is not quantified in XRD and hence FTIR is better tool for addressing the same. The FTIR spectrum recorded between 4000-400 cm^{-1} is shown in Fig. 2a. The IR spectrum of CeO_2 nanoparticles shows a broad band at 3450 and at 1670 cm^{-1}, which are signature of hydroxyl stretching frequency and bending vibration corresponding to water [37]. This can be due to the absorbed hydroxide on the nanoparticles due to their high reactivity. The bands located at 730 cm^{-1} can be due to the Ce-O-Ce bending vibration. Peak at 1040 cm^{-1} is from C-O stretching vibration [38]. A peak around 1540 cm^{-1} corresponds to the vibrational stretching band of CO_2 that might be due to the unescaped CO_2 produced during combustion. A peak at 475 cm^{-1} corresponds to Ce-O stretching and peaks at 1040 and at 1385 cm^{-1} correspond to stretching vibrations of C-O and C=O, respectively [39]. It is thereby concluded that the organic species, hydroxyl ions are present on the surface and C-O may be trapped inside the pores present in the synthesized materials. Our synthesis conditions were restricted to low temperature of 500 ºC and as fuel (BM seeds) are rich in polypeptides and protienase-carbon need high temperature of more than 700 ºC for decomposition of the C-O or C=O species.

Diffuse reflectance (D-R) spectra: The Kubelka-Munk plots are obtained using the UV-visible diffuse reflectance spectra of CeO_2 nanoparticles (Fig. 2b). The reflectance starts to drop around 400 nm for all three samples. Optical band-gap (E_g) of these nanoparticles was estimated by employing Kubelka-Munk (K-M) model. Initially, the f(R) and the energy were estimated from the following equations [40]:

$$F(R_\infty) = \frac{(1-R_\infty)^2}{2R_\infty} \quad (1)$$

and

$$E = h\nu = \frac{hc}{\lambda}\text{Joules} = \frac{1240}{\lambda}\text{eV} \quad (2)$$

where, R_∞ refers to the reflection coefficient of the sample, λ the corresponding wavelength. The interception of the slope-with the *x*-axis gives the energy of the nanoparticles and value increases from 3 to 3.16 eV with decreasing fuel content. These values were in agreement with the expected bandgap of CeO_2.

Morphological studies: The surface morphology of CeO_2 nanoparticles was characterized by scanning electron microscope and the results are shown in Fig. 3. The porous network observed at micron level can be due to escaping gases (CO_2 and NO_2) released during the combustion synthesis. The escaping gases cause swelling of the materials and results in the formation of pores in the materials (honeycomb structure) (mean size 18-30.4 nm). The particles are connected to each other to form irregular porous size and shapes (sphere like shaped with less agglomeration) [41]. The 'Ce 'and 'O' elemental analysis

TABLE-1
CRYSTALLOGRAPHIC PARAMETERS OBTAINED FROM RIETVELD REFINEMENT

Space group: $Fm\bar{3}m$					
Atom	X	Y	Z	Biso (thermal displacement)	Occupancy
Ce	0.00000	0.00000	0.00000	0.41382	0.50366
O	0.25000	0.25000	0.25000	1.69445	1.00000
Bond distances: Ce–O = 2.345 Å, Ce–Ce = 3.829 Å, O–O = 2.707 Å			Bond angles: Ce–O–Ce = 109.47°, O–Ce–O = 70.52°		

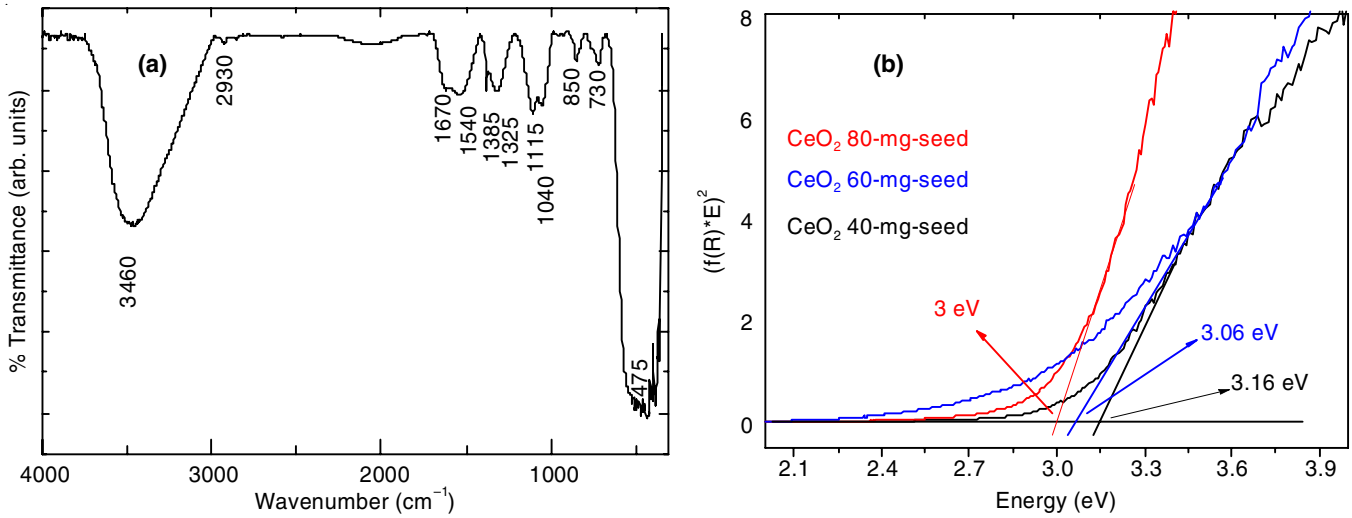

Fig. 2. FTIR spectra (a) and Kubelka Munk plots from Diffuse Reflectance Spectra (b) for the synthesized ceria

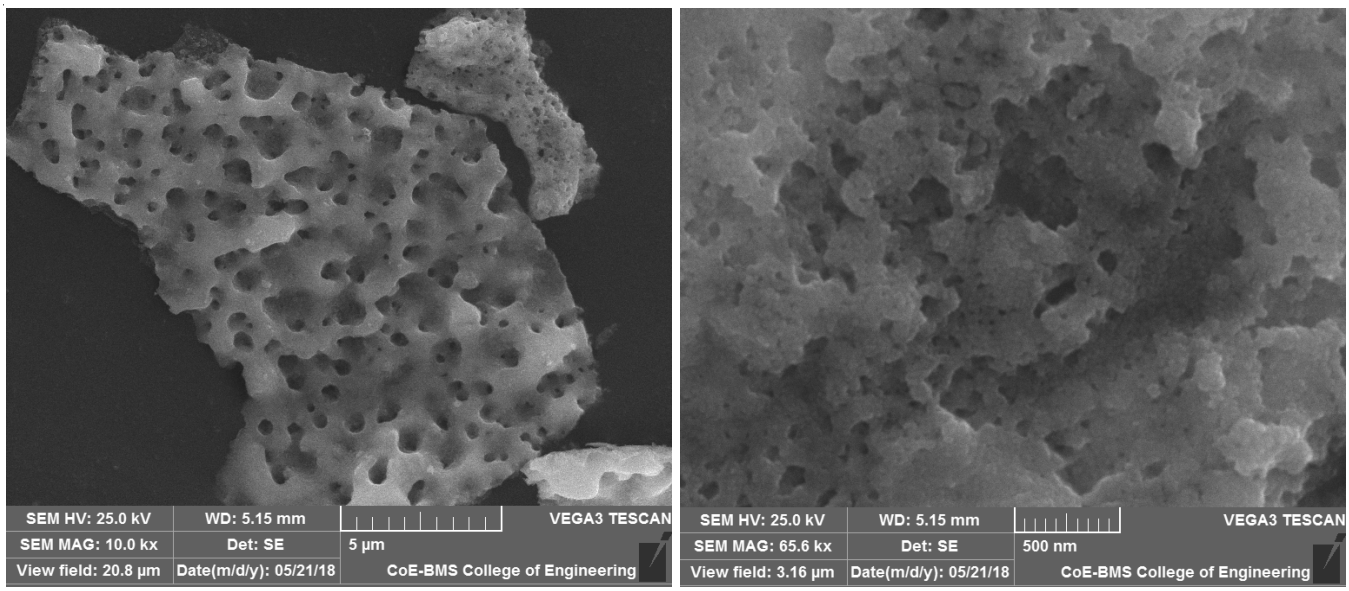

Fig. 3. SEM images of CeO_2 nanoparticles

of the samples was performed by EDAX using X-rays working at 25 kV. From the EDAX spectrum (Fig. 4), it is confirmed that there is a presence of 'Ce 'and 'O'. Further, the absence of other elements in the spectrum indicates the purity of the sample.

TEM studies of green synthesized CeO_2 nanoparticles reveals that the particles are connected with each other to form long chain with irregular size as well as shapes as shown in Fig. 5a. However higher resolution images confirm sphere like particles with size varying between 3 to 5 nm (Fig. 5b). The spacing between the lines of HRTEM image is around 0.27 nm which corresponds to the 200 orientation of the CeO_2 crystal. The electron diffraction image was further analyzed using the CrysTBox software [42] the *hkl* reflections generated from the image analysis matches with the once expected for the CeO_2 (Fig. 5d). Further diffraction pattern was simulated using the same software and is shown in the inset of Fig. 4b, the pattern obtained matches with XRD obtained from the powder diffraction in Fig. 1a. From the electron diffraction ring pattern it confirms that the nanoparticles are polycrystalline in nature and are good crystalline. The agglomeration can be due to the carbon residual which may get coated on to the nanoparticles forming surface layer interconnecting the particles. The carbon coated however, has dual effect, increase in the photocatalytic activity and reduction in the surface area.

BET surface area: Fig. 6a display the N_2 adsorption-desorption isotherms, it is a typical IUPAC type IV pattern with of a narrower hysteresis loop [43], the surface area obtained is 98.1 m^2/g. The pore size of 11.5 nm was determined from the Barret-Halenda (B-H) pore size distribution plot. The agglomeration of the particles and presence of carbon on the particles may be the reason for the decreased surface area [44]. The surface area of the ceria nanoparticles can be tuned upto 300 m^2/g, in present case, it is believed the presence of carbon in the grain boundary may result in the interconnection of the grains thereby reducing the total surface area.

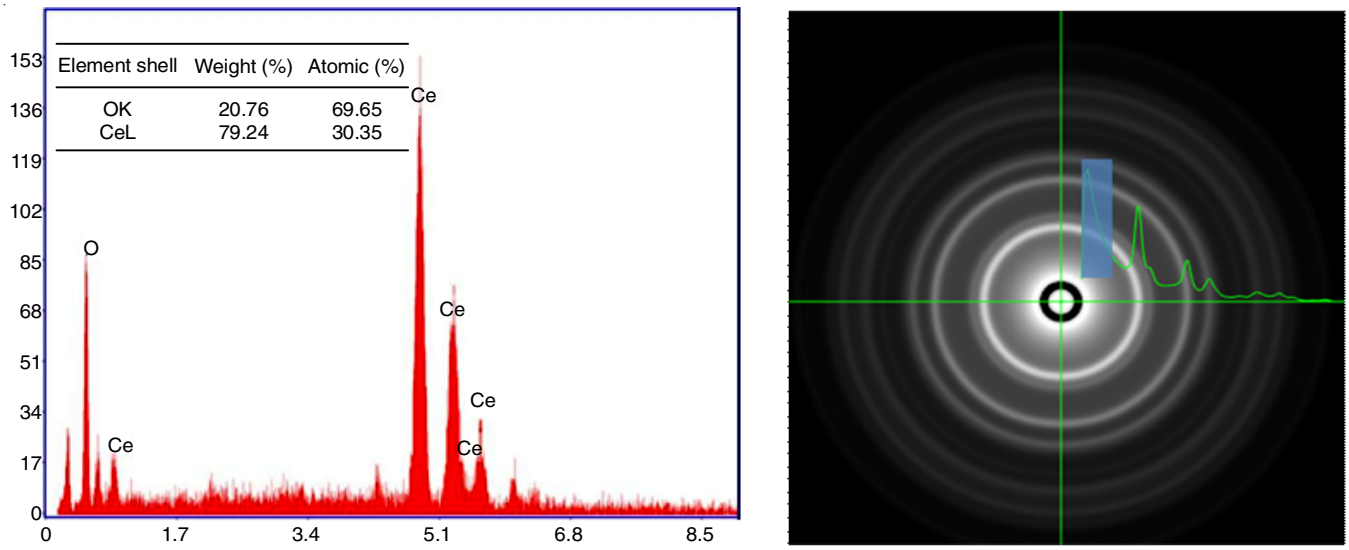

Fig. 4. EDAX spectra obtained on the synthesized sample (left). The calculated diffraction pattern from TEM matches with the one obtained on lab powder diffractometer

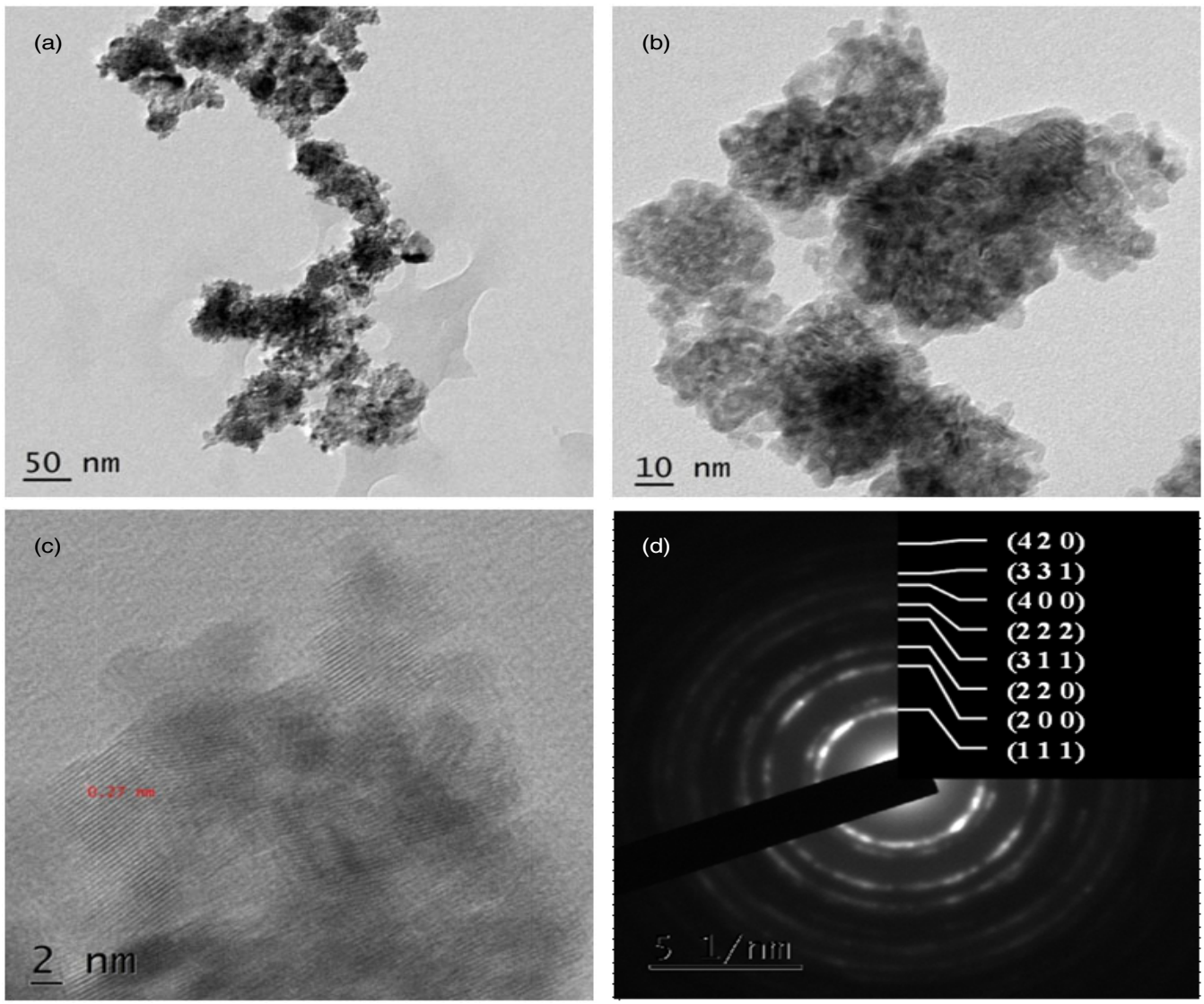

Fig. 5. (a) and (b) TEM images obtained for the synthesized CeO_2 nanoparticles using 60 mg seed as fuel. (c) HRTEM image with d spacing 0.27 nm corresponding to 200 miller plane and (d) miller indecies for each diffraction ring as obtained from analysis using CrysTBox

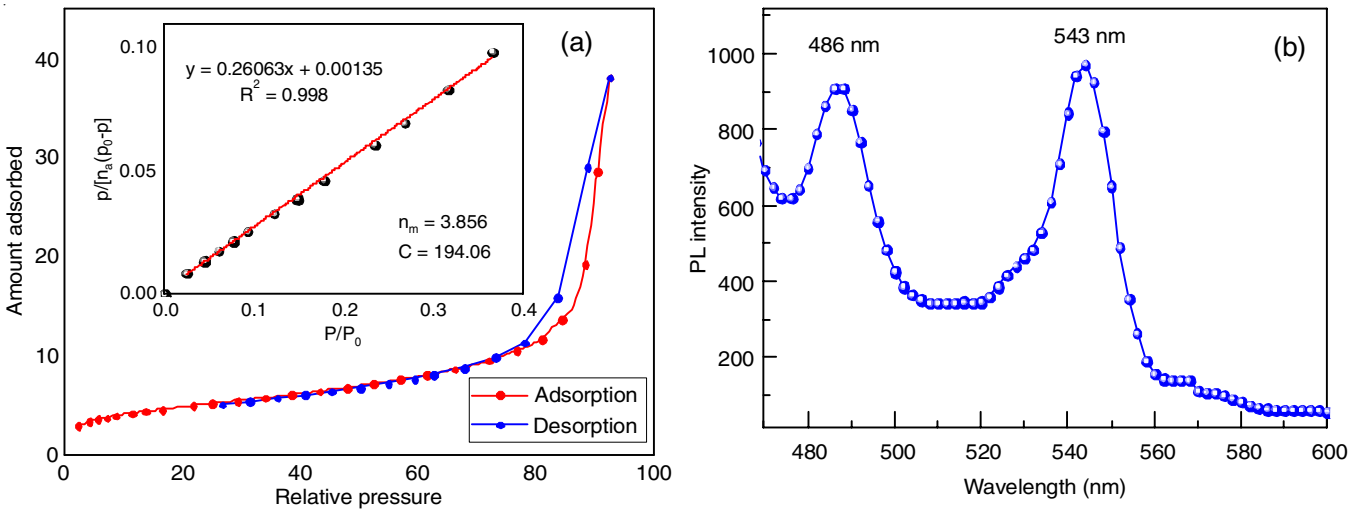

Fig. 6. BET N_2 adsorption-desorption curves (a) and photoluminescence spectra (b)

Photoluminescence studies: Fig. 6b displays the photoluminescence spectra of CeO_2 nanoparticles synthesized by solution combustion method using *Butea monosperma* seed as fuel. The nanoparticles are excited with a wavelength of 398 nm resulting in an emission peaks at 486 nm (2.6 eV) corresponds to blue-green emission band and 543 nm (2.33 eV) more precisely corresponds to green emission band [45,46]. These obtained emissions can be assignedto the transition of electrons from 4f band of cerium to the 2p band of 'O". While the emission band ranging between 486 to 543 nm can be the result of defects, including vacancies in the crystal with electronic energy levels below the 4f band.

Photocatalytic properties: Synthesized CeO_2 nanoparticles were used as photocatalyst to examine the degradation of methylene blue under UV source. Aliquot (3 mL) was withdrawn after every 10 min time interval from the batch reactor, centrifuged and absorption of the degraded dye was recorded. The UV-visible absorption curves and the degradation percentage calculated are shown in Fig. 7, the degradation kinetics are studied using the pseudo-first order reaction relation and the rate constant obtained for our studies is around 0.522 [47]. Adsorbed dye molecules did not degrade faster, because the catalyst load and light intensity is constant. If the concentration of dye was more than the penetrating power of light will be less andthe resulting production of superoxide and hydroxyl radicals will be less.

Biodiesel production and evaluation of fuel properties: After completion of transesterification, 84% of biodiesel yield was obtained. Further, the fuel properties of biodiesel were evaluated according ASTM standard. Table-2 shows the fuel properties biodiesel within the standard limit. Cotton seed oil has high viscosity and is 12 times higher than diesel fuel this causes the deposition of carbon on the injector and also poor fuel atomization, making it achallenge to be used in diesel engine. By transesterification viscosity of the oil is reduced. Density and viscosity of biodiesel are found to be 5.2 *c*St and 884 kg/m^3, respectively. The flash point of biodiesel is 168 ºC and is within the range of standard, is also safer for transp-

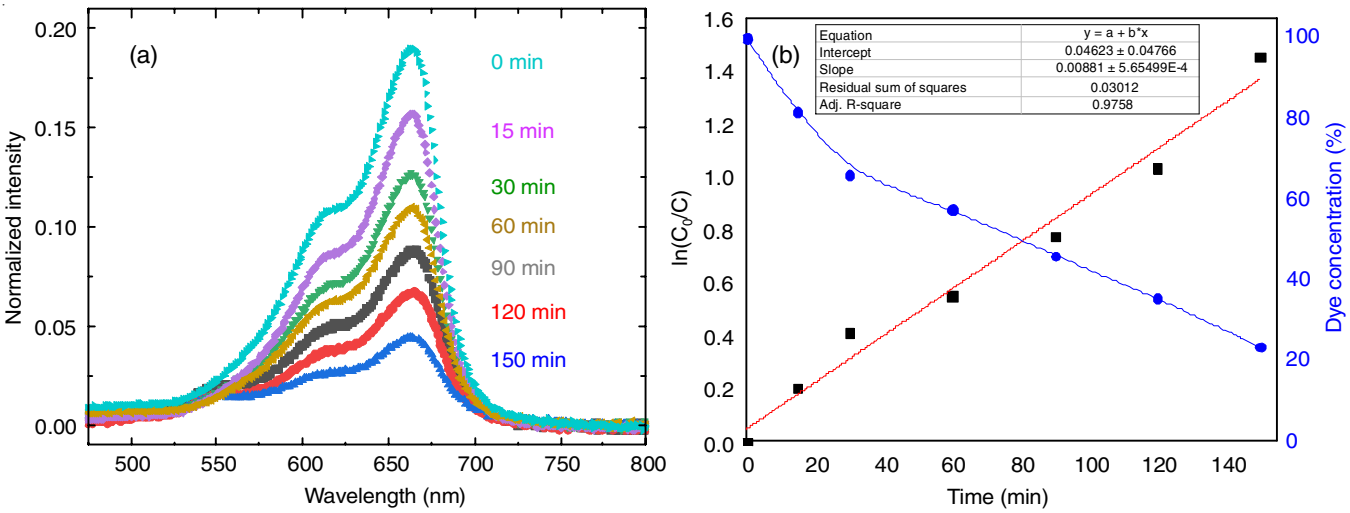

Fig. 7. UV-vis spectra on the dye drawn at different time interval (a). The analysis of dye degradation data using linear fitting along with variation of dye concentration with irradiation time (b)

TABLE-2
FUEL PROPERTIES OF BIODIESEL

Properties	ASTM standard	Biodiesel produced using synthesized CeO_2Nps	Diesel	ASTM-6751 biodiesel
Flash point (°C)	D4052	168	60	> 130
Density at 15 °C (kg/m^3)	D93	884	834	–
Copperstrip corrosion, 50 °C, 3h	D130	1a	1a	No. 3 max
Viscosity at 40 °C (cSt)	D445	5.2	2.6	1.9-6.0
Acid value (mg KOH/g)	D664	0.2	0.20	0.50 max

ortation and storage. Copper strip corrosion test value determined as per the ASTM D130 was found to be 1a and lies within the accepted values. The acid value found to be 0.2 Mg KOH/g. Therefore, all outcomes in this work showed that CeO_2 nanoparticles shows greater catalytic activity for biodiesel production from the cotton seed oil.

Antibacterial studies: The zone of inhibition was carried out by Agar well diffusion method the results are summarized in Table-3. The studies revealed that ceria nanoparticles successfully inhibited the growth of test organisms with different sized zones of inhibition. Present investigations revealed an encouraging result on the *in vitro* efficacy of CeO_2 compared to standard drug. It was observed that CeO_2 has showed selective antimicrobial activity against the Gram-positive organism, whereas Gram-negative organism is resistant to all synthesized nanoparticles. From these trials, it is confirmed good antimicrobial activity of the synthesized ceria nanoparticles.

TABLE-3
ANTIBACTERIAL ACTIVITY OF NANOPARTICLES

Nanoparticles loading per mL	Zone of inhibition (mm)		
	Staphylococcus aureus	*Pseudomonos aeruginosa*	*Escherichia coli*
CeO_2, 100 µg	9 ± 0.25	8 ± 0.19	Not seen
CeO_2, 200 µg	10 ± 0.13	9 ± 0.11	Not seen
Ciproflaxacin 10 µg	16 ± 0.09	15 ± 0.08	4 ± 0.15

Conclusion

Ceria (CeO_2) nanoparticles were synthesized using *Butea monosperma* seed powder as fuel by solution combustion synthesis along with cerium nitrate. The crystallite size can be tuned between 8 to 15 nm using appropriate seed concentration, the crystallite size increases with increasing seed concentration. TEM and FTIR results complement that carbon residue binds the nanoparticles also helps in increase in the photocatalytic activity. The nanoparticles with surface area of 98.1 m^2/g showed 85% of photodegradation of methylene blue dye under UV radiation. The synthesized ceria nanoparticles are for the first time demonstrated as the possible photocatalysts for the conversion of cotton seed oil into biodiesel with a conversion efficiency of around 84%. Thereby, it is demonstrated that ceria nanoparticles obtained through combustion synthesis to exhibit excellent photocatalytic activity for biodiesel production, antibacterial properties under the optimum conditions.

ACKNOWLEDGEMENTS

One of the authors, GER acknowledge Udayabhanu and Shashank for their assistance in UV and photoluminescence characterization of the samples. The same also thank SSES for the financial support, CEO and Director of SIT for their constant encouragement extended during his doctoral studies. Another author, MC acknowledge the VGST funding under SMYSR/GRD-583/2016-17.

CONFLICT OF INTEREST

The authors declare that there is no conflict of interests regarding the publication of this article.

REFERENCES

1. J.P. Holgado, R. Alvarez and G. Munuera, *Appl. Surf. Sci.*, **161**, 301 (2000); https://doi.org/10.1016/S0169-4332(99)00577-2
2. M.C. Arnold, A.R. Badireddy, M.R. Wiesner, R.T. Di Giulio and J.N. Meyer, *Arch. Environ. Contam. Toxicol.*, **65**, 224 (2013); https://doi.org/10.1007/s00244-013-9905-5
3. F. Perera, *Int. J. Environ. Res. Public Health*, **15**, 16 (2018); https://doi.org/10.3390/ijerph15010016
4. R. Heede, *Climatic Change*, **122**, 229 (2014); https://doi.org/10.1007/s10584-013-0986-y
5. A. Sundaresan and C.N.R. Rao, *Nano Today*, **4**, 96 (2009); https://doi.org/10.1016/j.nantod.2008.10.002
6. M. Zarezadeh Mehrizi, S. Ahmadi, R. Beygi and M. Asadi, *Russ. J. Non-Ferrous Met.*, **59**, 111 (2018); https://doi.org/10.3103/S1067821218010170
7. K. Sohlberg, S.T. Pantelides and S.J. Pennycook, *J. Am. Chem. Soc.*, **123**, 6609 (2001); https://doi.org/10.1021/ja004008k
8. T. Masui, H. Hirai, N. Imanaka, G. Adachi, T. Sakata and H. Mori, *J. Mater. Sci. Lett.*, **21**, 489 (2002); https://doi.org/10.1023/A:1015342925372
9. W. Lin, Y. Huang, X. Zhou and Y. Ma, *Int. J. Toxicol.*, **25**, 451 (2006); https://doi.org/10.1080/10915810600959543
10. A. Kopia, K. Kowalski, M. Chmielowska and C. Leroux, *Surf. Sci.*, **602**, 1313 (2008); https://doi.org/10.1016/j.susc.2007.12.041
11. N. Agasti, M.A. Astle, G.A. Rance, J.A. Fernandes, J. Dupont and A.N. Khlobystov, *Nano Lett.*, **20**, 1161 (2020); https://doi.org/10.1021/acs.nanolett.9b04579
12. Z. Xiong, Z. Lei, Z. Xu, X. Chen, B. Gong, Y. Zhao, H. Zhao, J. Zhang and C. Zheng, *Biochem. Pharmacol.*, **18**, 53 (2017); https://doi.org/10.1016/j.jcou.2017.01.013
13. F.T. Li, J. Ran, M. Jaroniec and S.Z. Qiao, *Nanoscale*, **7**, 17590 (2015); https://doi.org/10.1039/C5NR05299H
14. W. Wen and J.-M. Wu, *RSC Adv.*, **4**, 58090 (2014); https://doi.org/10.1039/C4RA10145F
15. X. Wang, M. Qin, F. Fang, B. Jia, H. Wu, X. Qu and A.A. Volinsky, *Ceram. Int.*, **44**, 4237 (2018); https://doi.org/10.1016/j.ceramint.2017.12.004
16. D. Parviz, M. Kazemeini, A.M. Rashidi and K.J. Jozani, *J. Nanopart. Res.*, **12**, 1509 (2010); https://doi.org/10.1007/s11051-009-9727-6
17. O.V. Kharissova, H.V.R. Dias, B.I. Kharisov, B.O. Perez and V.M.J. Perez, *Cell Press*, **31**, 240 (2013); https://doi.org/10.1016/j.tibtech.2013.01.003

18. I. Hussain, N.B. Singh, A. Singh, H. Singh and S.C. Singh, *Biotechnol. Lett.*, **38**, 545 (2016); https://doi.org/10.1007/s10529-015-2026-7
19. B.S. Rohini, H. Nagabhushana, G.P. Darshan, R.B. Basavaraj, S.C. Sharma and R. Sudarmani, *Appl. Nanosci.*, **7**, 815 (2017); https://doi.org/10.1007/s13204-017-0611-x
20. L.S. Reddy Yadav, K. Manjunath, B. Archana, C. Madhu, H. Raja Naika, H. Nagabhushana, C. Kavitha and G. Nagaraju, *Eur. Phys. J. Plus*, **131**, 154 (2016); https://doi.org/10.1140/epjp/i2016-16154-y
21. J. Malleshappa, H. Nagabhushana, S.C. Sharma, Y.S. Vidya, K.S. Anantharaju, S.C. Prashantha, B.D. Prasad, H.R. Naika, K. Lingaraju and B.S. Surendra, *Spectrochim. Acta A Mol. Biomol. Spectrosc.*, **149**, 452 (2015); https://doi.org/10.1016/j.saa.2015.04.073
22. M. Feyzi and Z. Shahbazi, *J. Taiwan Inst. Chem. Eng.*, **71**, 145 (2017); https://doi.org/10.1016/j.jtice.2016.11.023
23. M. Feyzi and L. Norouzi, *Renew. Energy*, **94**, 579 (2016); https://doi.org/10.1016/j.renene.2016.03.086
24. E.A. Faria, J.S. Marques, I.M. Dias, R.D.A. Andrade, P.A.Z. Suarez and A.G.S. Prado, *J. Braz. Chem. Soc.*, **20**, 1732 (2009); https://doi.org/10.1590/S0103-50532009000900023
25. Q. Zhou, H. Zhang, F. Chang, H. Li, H. Pan, W. Xue, D.-Y. Hu and S. Yang, *J. Ind. Eng. Chem.*, **31**, 385 (2015); https://doi.org/10.1016/j.jiec.2015.07.013
26. M. Raghavendra, K.V. Yatish and H.S. Lalithamba, *Eur. Phys. J. Plus*, **132**, 358 (2017); https://doi.org/10.1140/epjp/i2017-11627-1
27. G. Baskar and S. Soumiya, *Renew. Energy*, **98**, 101 (2016); https://doi.org/10.1016/j.renene.2016.02.068
28. B. Gurunathan and A. Ravi, *Bioresour. Technol.*, **188**, 124 (2015); https://doi.org/10.1016/j.biortech.2015.01.012
29. A. Pathak, K. Vajpai and S.K.Vajpai, *Biomed. Pharmacol. J.*, **5**, 45 (2012); https://doi.org/10.13005/bpj/319
30. P. Tiwari, S. Jena and P.K. Sahu, *Acta Sci. Pharm. Sci.*, **3**, 19 (2019).
31. M. Srivastava, S. Srivastava and S. Khatoon, *Nat. Prod. Sci.*, **8**, 83 (2002).
32. I.B. Bankovic-Ilic, O.S. Stamenkovic and V.B. Veljkovic, *Renew. Sustain. Energy Rev.*, **16**, 3621 (2012); https://doi.org/10.1016/j.rser.2012.03.002
33. N.G. Udayabhanu, G. Nagaraju, H. Nagabhushana, R.B. Basavaraj, G.K. Raghu, D. Suresh, H. Rajanaika and S.C. Sharma, *Cryst. Growth Des.*, **16**, 6828 (2016); https://doi.org/10.1021/acs.cgd.6b00936
34. K.V. Yatish, H.S. Lalithamba, R. Suresh and H.K.E. Latha, *Renew. Energy*, **147**, 310 (2020); https://doi.org/10.1016/j.renene.2019.08.139
35. P.C. Trussell, E.A. Baird, D. Beall and G.A. Grant, *Can. J. Res.*, **38**, 61 (1944); https://doi.org/10.1139/cjr47e-002
36. National Committee for Clinical Laboratory Standards N. M02-A12, Performance Standards for Antimicrobial Disk Susceptibility Tests; Approved Standard, Ed. 12, pp. 35-73 (2015).
37. P. Periyat, F. Laffir, S.A.M. Tofail and E. Magner, *RSC Adv.*, **1**, 1794 (2011); https://doi.org/10.1039/c1ra00524c
38. T.N. Ravishankar, T. Ramakrishnappa, G. Nagaraju and H. Rajanaika, *ChemistryOpen*, **4**, 146 (2015); https://doi.org/10.1002/open.201402046
39. A.C. Tas, P.J. Majewski and F. Aldinger, *J. Am. Ceram. Soc.*, **83**, 2954 (2000); https://doi.org/10.1111/j.1151-2916.2000.tb01666.x
40. A.J. Deotale and R.V. Nandedkar, *Mater. Today Proc.*, **3**, 2069 (2016); https://doi.org/10.1016/j.matpr.2016.04.110
41. M. Farahmandjou, M. Zarinkamar and T.P. Firoozabadi, *Rev. Mex. F'ýsica*, **62**, 496 (2016).
42. M. Klinger and A. Jäger, *J. Appl. Cryst.*, **48**, 2012 (2015); https://doi.org/10.1107/S1600576715017252
43. Q.R. Fang, T.A. Makal, M.D. Young and H.C. Zhou, *Comments Inorg. Chem.*, **31**, 165 (2010); https://doi.org/10.1080/02603594.2010.520254
44. A. Wheeler, *Adv. Catal.*, **3**, 249 (1951); https://doi.org/10.1016/S0360-0564(08)60109-1
45. M.M. Ali, H.S. Mahdi, A. Parveen and A. Azam, *AIP Conf. Proc.*, **1953**, 030044 (2018); https://doi.org/10.1063/1.5032379
46. I.N. Bazhukova, S.Y. Sokovnin, V.G. Ilves, A.V. Myshkina, R.A. Vazirov, N. Pizurova and V.V. Kasyanova, *Opt. Mater.*, **92**, 136 (2019); https://doi.org/10.1016/j.optmat.2019.04.021
47. K.M. Lee, S.B. Abd Hamid and C.W. Lai, *J. Nanomater.*, **2015**, 940857 (2015); https://doi.org/10.1155/2015/940857